Geospatial Machine Learning for Predicting Flash Flood Response at Ungauged Appalachian Watersheds: Terrain, Soil, and Land Cover Controls

Sujan Bhattarai

Independent Researcher

Corresponding author: sujanbhattarai.jr@gmail.com

Abstract

Flash floods remain among the deadliest weather hazards in the United States, yet the majority of flood-prone watersheds in the Appalachian region lack streamflow monitoring. Predicting flood response characteristics at these ungauged sites requires understanding which landscape properties control hydrologic behavior. This study evaluates whether geospatial basin descriptors derived from high-resolution terrain, soil, and land cover datasets can predict seven flood response metrics across 49 gauged Appalachian watersheds spanning seven states (Virginia, West Virginia, North Carolina, Tennessee, Kentucky, Georgia, and Pennsylvania). Predictor variables were extracted from the USGS 3D Elevation Program (10 m), the National Land Cover Database (30 m), and the NRCS Soil Data Access service. Four model families were compared using leave-one-out spatial cross-validation: regularized linear models (Ridge, ElasticNet), tree-based models (Random Forest, XGBoost), and Gaussian Process Regression (GPR) with multiple kernel configurations. Results show that GPR with a Matern 1.5 kernel achieves the highest predictive skill for the Q95 discharge ratio (R-squared = 0.46) and mean rise rate (R-squared = 0.73), while regularized linear models perform comparably or better for other targets. Flashiness index and coefficient of variation of annual peaks are not predictable from static geospatial descriptors (R-squared approximately equal to 0), indicating that these properties depend on storm characteristics rather than landscape attributes. Spearman correlation analysis identifies basin relief (rho = -0.58, $p < 0.001$) and drainage area (rho = -0.42, $p < 0.01$) as the strongest correlates of flood response. SHAP-based feature importance analysis confirms that terrain properties dominate across most targets, contributing 42 to 69 percent of total importance. GPR prediction intervals show well-calibrated uncertainty, with observed 95 percent coverage ranging from 88 to 95 percent across targets. These findings suggest that geospatial machine learning can

provide moderate predictive skill for flood magnitude indicators at ungauged Appalachian sites, but flashiness metrics require dynamic storm-event information that static basin descriptors cannot capture.

Keywords: *flash flood susceptibility; ungauged basins; geospatial machine learning; Gaussian process regression; SHAP interpretability; Appalachian hydrology; uncertainty quantification; terrain analysis*

1. Introduction

1.1 Geospatial Knowledge in Hydrology

Geospatial data have become central to modern hydrology because the physical processes that control flood generation operate across spatial scales that can only be characterized through spatially distributed datasets (Vieux, 2016). The partitioning of rainfall into infiltration and surface runoff depends on terrain slope, soil depth, hydraulic conductivity, and land cover type. These properties vary across a watershed and can be quantified through raster datasets such as digital elevation models, gridded soil surveys, and satellite-derived land cover maps (Dunne and Leopold, 1978; Daly et al., 2008). The USGS 3D Elevation Program provides 10-meter gridded elevation data across the continental United States, from which slope, relief, and topographic wetness index can be computed at scales relevant to flash flood generation (Gesch et al., 2018). The National Land Cover Database provides 30-meter land cover classification for the country (Dewitz, 2023). The NRCS gridded Soil Survey Geographic database provides soil hydraulic properties, including saturated conductivity, available water capacity, and depth to bedrock, at 10-meter resolution (Soil Survey Staff, 2024). The combination of these raster datasets with vector representations of watershed boundaries and stream networks has enabled a transition from lumped, basin-averaged hydrologic analysis to spatially explicit characterization of the landscape properties that control runoff response (Falcone, 2011). For ungauged basins, where no discharge observations exist, geospatial datasets are the primary available source of information about basin properties (Sivapalan et al., 2003; Hrachowitz et al., 2013). The ability to extract useful predictors from these datasets and connect them to observed flood behavior at gauged locations is a necessary step toward extending flood risk assessment to the thousands of

unmonitored watersheds where communities remain at risk. A recent review of geospatial artificial intelligence applications in hydrology identified more than 1,300 publications over the last two decades, noting that GeoAI has shown advantages in nonlinear modeling, integration of multiple data sources, and high prediction accuracy, but that low physical interpretability and limited model generalization remain major drawbacks (Gonzales-Inca et al., 2022).

1.2 Geospatial Controls on Flood Response

The physical properties of a watershed control how it responds to rainfall. Terrain morphometry determines how water moves across the landscape: steep slopes speed up overland flow and reduce the time available for infiltration, while basin relief controls the gravitational energy available for runoff generation (Beven and Kirkby, 1979; Wolock and McCabe, 1995). Soil hydraulic properties, including saturated hydraulic conductivity and depth to bedrock, control the split between infiltration and surface runoff. In the Appalachian region, shallow soils over fractured bedrock are a primary driver of flash flood generation through the saturation-excess runoff mechanism (Gourley et al., 2017; Tao and Barros, 2013).

Land cover affects flood response through interception, infiltration, and surface roughness. Forest canopies intercept rainfall before it reaches the soil, reducing water available for runoff (Calder, 1990). Developed and impervious surfaces reduce infiltration capacity and increase runoff volume and peak discharge (Booth and Jackson, 1997). Gannon et al. (2022) used the Richards-Baker Flashiness Index to examine controls on watershed flashiness across the continental United States and found that flashiness was not well organized by drainage area at continental scales; instead, controls varied by hydroclimatic region.

1.3 Geospatial Machine Learning for Flood Prediction

The use of geospatial features as predictors in flood modeling has grown as machine learning methods have shown the ability to learn relationships between basin characteristics and hydrologic response. Flood susceptibility mapping studies have used terrain derivatives such as slope, elevation, topographic wetness index, and distance to streams as inputs for classification models including Random Forest, XGBoost, and convolutional neural networks (Pradhan et al., 2023; Aydin and Iban, 2023). These studies report that elevation, slope, and drainage-related features rank among the most important predictors across different geographic settings. At the basin scale, the CAMELS dataset (Addor et al., 2017) and the GAGES-II dataset (Falcone, 2011) provide precomputed geospatial attributes for hundreds of gauged watersheds across the United States, which has made large-sample studies relating basin characteristics to streamflow behavior possible. Kratzert et al. (2019) used CAMELS basin attributes as static inputs to LSTM models and showed that including geospatial information improves the transfer of models to ungauged basins. Gannon et al. (2022) used GAGES-II attributes to examine controls on watershed flashiness and found that the importance of different geospatial predictors changes by hydroclimatic region, with subsurface properties dominating in some areas and topographic properties dominating in others. Rojas Aldana et al. (2021) used basin physiographic features alongside precipitation characteristics to predict flood peaks in ungauged basins and showed that static catchment attributes carry more predictive signal than dynamic storm variables for low-to-moderate flood events. Despite this progress, most geospatial flood studies have focused on pixel-level susceptibility classification rather than prediction of continuous flood response metrics at the basin scale, and few have used uncertainty-aware methods such as Gaussian Process Regression for the ungauged prediction problem in specific flood-prone regions.

1.4 Interpretability and Uncertainty

SHAP-based interpretability analysis applied to flood susceptibility models has confirmed the importance of terrain factors across multiple settings. Distance to streams, topographic wetness index, and elevation have been identified as the top three predictors in studies in Iran, South Korea, and the Tibetan Plateau (Pradhan et al., 2023; Aydin and Iban, 2023; Lundberg and Lee, 2017). However, these studies use binary classification with large pixel-level datasets rather than predicting continuous flood response metrics at the basin scale. Whether the same feature importance rankings hold when predicting basin-scale flood characteristics such as flashiness, peak ratios, and recession behavior has not been tested.

Uncertainty quantification in flood prediction remains an open problem (Beven, 2016). Most machine learning models used in flood studies produce point predictions without confidence bounds. Gaussian Process Regression (GPR) provides a Bayesian approach to uncertainty estimation that addresses this gap. Sun et al. (2014) applied GPR to monthly streamflow forecasting across 438 MOPEX basins and showed that GPR provides accurate predictions with meaningful prediction intervals. Kohanpur et al. (2023) used physics-informed GPR for urban flood forecasting with uncertainty bounds. For ungauged basin prediction, calibrated uncertainty estimates matter because emergency managers need to know not only the expected flood response but also how much confidence to place in that prediction.

1.5 Scope and Contributions

This study addresses four questions. First, to what extent can geospatial basin descriptors derived from high-resolution terrain, soil, and land cover data predict flash flood response characteristics at ungauged Appalachian watersheds? Second, which geospatial feature groups exert the strongest control on different aspects of flood response? Third, does machine learning provide meaningful improvement over regularized linear models at the available sample size? Fourth,

can Gaussian Process Regression provide well-calibrated uncertainty estimates for flood response predictions at ungauged sites?

This work is an extension of a companion study (Bhattarai, 2026) that examined temporal ML-based flood forecasting at nine gauged Appalachian stations using hourly USGS streamflow and NOAA AORC precipitation data with SHAP-based physical consistency testing. That study addressed the temporal prediction problem: given a basin with historical observations, can ML forecast discharge hours into the future? The present study addresses the spatial prediction problem: given a basin with no discharge observations, can its flood response characteristics be predicted from landscape properties alone? The companion study found that Random Forest outperformed LSTM at 12- and 24-hour lead times, that discharge lag features dominate SHAP importance at all leads, and that medium-window antecedent precipitation and soil moisture proxy importance increase with lead time in ways consistent with saturation-excess runoff theory. The present study asks whether the same geospatial properties that control temporal flood behavior within individual basins also explain the spatial variation in flood response across basins. Together, the two studies are intended to cover the prediction needs for both gauged and ungauged basins in the Appalachian region.

2. Study Area and Data

2.1 Study Region

The study encompasses 49 USGS gauging stations across the central and southern Appalachian region, spanning seven states: Virginia (8 stations), West Virginia (7), North Carolina (12), Tennessee (9), Kentucky (5), Georgia (3), South Carolina (1), and Pennsylvania (5). The stations cover a range of basin sizes from 65 to 9,520 square kilometers and elevations from 172 to 1,170 meters above sea level. The region is characterized by steep, forested terrain with shallow soils over crystalline and sedimentary bedrock, producing rapid hydrologic response to intense rainfall (Smith et al., 2011).

Flash floods in the study area are driven by three primary meteorological mechanisms: slow-moving mesoscale convective systems during summer, tropical cyclone remnants during late summer and autumn, and frontal precipitation systems during spring (Gourley et al., 2017; Woods et al., 2023). The 25-year study period (2000 to 2024) encompasses multiple catastrophic flood events, including the remnants of Hurricanes Frances and Ivan in 2004 and Hurricane Helene in September 2024.

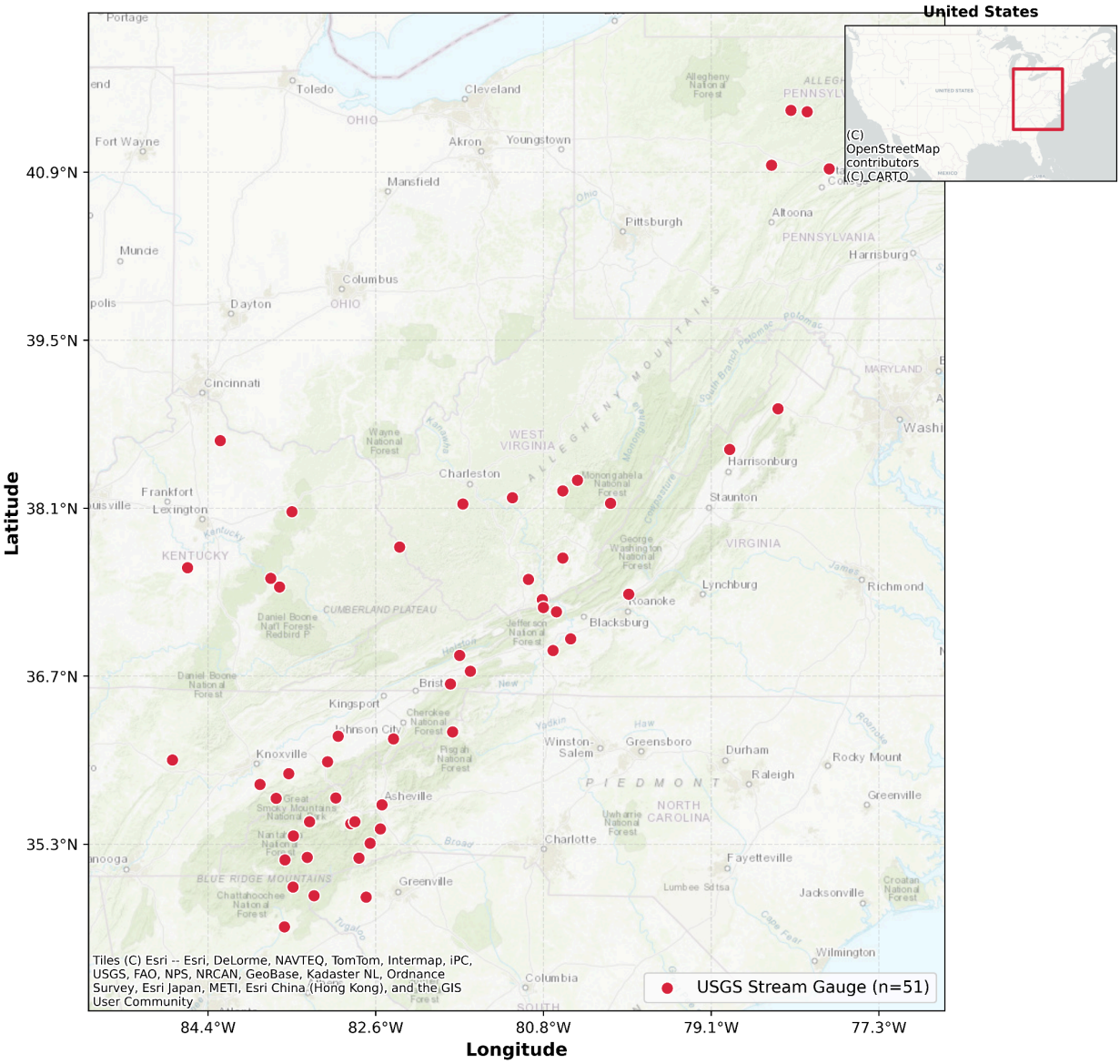

Figure 1. Study area showing 49 USGS gauging stations across the Appalachian region, colored by flashiness index. Gray crosses indicate stations excluded due to insufficient data.

2.2 Streamflow Data

Daily mean discharge records were obtained from the USGS National Water Information System (NWIS) for the period January 2000 through December 2024 (USGS, 2024). Of the 52 stations initially selected, 49 had sufficient record length (more than five years of valid daily

data) for computation of flood response metrics. Record lengths across the 49 retained stations ranged from 8 to 25 years, with 35 stations having the full 25-year record.

2.3 Flood Response Metrics

Seven flood response metrics were computed from each station's daily discharge record. The flashiness index was calculated following Baker et al. (2004) as the sum of absolute day-to-day changes in discharge divided by total discharge. The Q95 and Q99 ratios were computed as the 95th and 99th percentile of daily discharge divided by the median discharge. The coefficient of variation of annual peak discharge measures interannual variability. Mean rise rate was computed as the average of all positive day-to-day discharge changes. Time to peak was estimated as the median duration from event onset to peak discharge. The recession constant was estimated by fitting exponential decay curves to the falling limbs of discharge events.

2.4 Geospatial Predictor Variables

Eleven geospatial predictor variables were selected based on physical relevance to flood generation. Terrain variables (mean basin slope, relief, and mean elevation) were derived from the USGS 3D Elevation Program (3DEP) 10-meter digital elevation model (Gesch et al., 2018). Soil properties (saturated hydraulic conductivity, clay fraction, and depth to bedrock) were obtained from the NRCS Soil Data Access service (Soil Survey Staff, 2020). Land cover fractions (forest cover and developed land) were computed from the 2021 National Land Cover Database at 30-meter resolution (Dewitz and USGS, 2023). Mean annual precipitation was estimated from the PRISM Climate Group 800-meter dataset (Daly et al., 2008). Drainage area was obtained from USGS site metadata, and drainage density was computed from the NHDPlus High Resolution stream network.

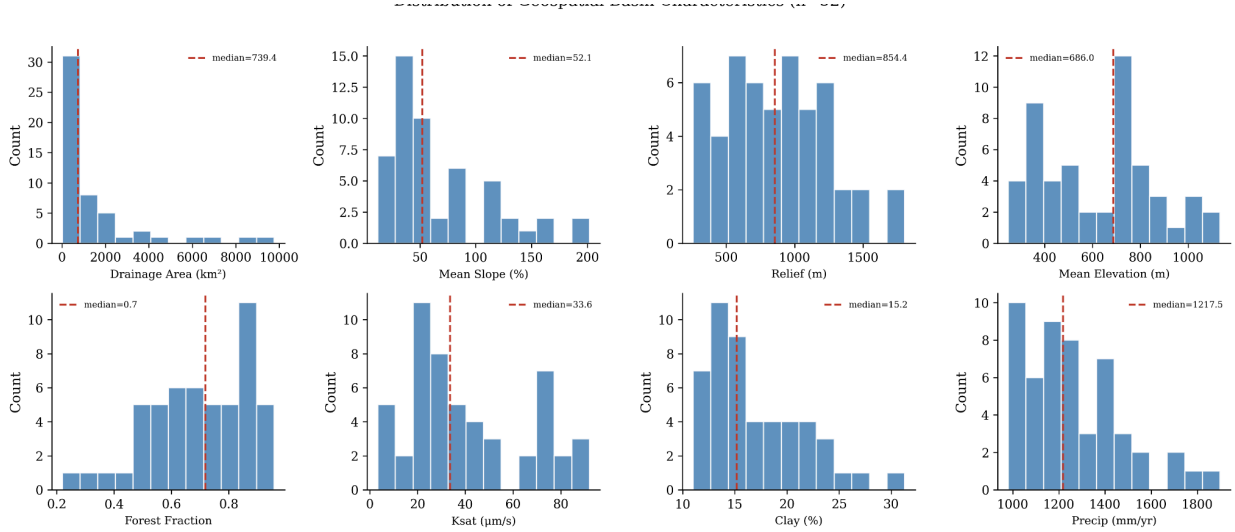

Figure 2. Distribution of geospatial basin characteristics across the 52 study stations. Red dashed lines indicate median values.

3. Methods

3.1 Feature Selection

An initial set of 11 predictor variables was assembled. Collinearity was assessed using pairwise Pearson correlation coefficients; no pairs exceeded the 0.80 threshold, and all 11 were retained. For each target variable, a target-specific feature subset was selected based on Spearman rank correlation. Features with absolute rho greater than 0.20 or p-value less than 0.10 were included in the ML models for that target, resulting in 4 to 7 features per target.

3.2 Machine Learning Models

Four model families were evaluated: Ridge regression (alpha = 10.0), ElasticNet (alpha = 0.1, L1 ratio = 0.5), Random Forest (200 trees, max depth = 3, min samples per leaf = 5), and XGBoost (100 trees, max depth = 2, learning rate = 0.05, L1 alpha = 2.0, L2 lambda = 5.0). All models were configured with strong regularization appropriate for the small-sample regime.

3.3 Gaussian Process Regression

Five kernel configurations were tested: radial basis function (RBF), Matern with nu = 1.5 and 2.5, Rational Quadratic, and a composite RBF plus linear kernel. Each kernel was combined with constant and white noise components. Hyperparameters were optimized by maximizing the log marginal likelihood with five random restarts.

3.4 Leave-One-Out Spatial Cross-Validation

All models were evaluated using leave-one-out cross-validation, in which each station is held out in turn and a prediction is made from geospatial features alone. This procedure

simulates the ungauged basin scenario. Performance was evaluated using R-squared, NSE, MAE, RMSE, and NRMSE.

3.5 Uncertainty Calibration

For GPR models, the fraction of held-out observations falling within one-sigma and two-sigma prediction intervals was computed. A well-calibrated model should have approximately 68 percent within one sigma and 95 percent within two sigma.

3.6 SHAP Feature Importance

SHAP values were computed using TreeSHAP applied to Random Forest models trained on the full dataset. Mean absolute SHAP values were aggregated by feature group to assess the relative contribution of terrain, soils, land cover, climate, and morphometry.

4. Results

4.1 Basin Characteristics

The 49 retained stations span a wide range of physiographic conditions (Figure 2). Drainage areas range from 65 to 9,520 square kilometers (median = 739 square kilometers). Mean basin slope ranges from 14 to 210 percent (median = 52 percent). Basin relief ranges from 74 to 1,580 meters (median = 854 meters). Forest cover fraction ranges from 0.22 to 0.95 (median = 0.70). Among the flood response metrics, flashiness index ranges from 0.19 to 0.61 (mean = 0.34, standard deviation = 0.10). The Q95 ratio ranges from 2.8 to 14.0 (mean = 5.7, standard deviation = 2.4).

4.2 Univariate Correlations

Spearman rank correlation analysis reveals distinct patterns of association between geospatial predictors and flood response metrics (Figure 3). The strongest correlations involve morphometric and terrain variables with mean rise rate: drainage area (rho = 0.81, $p < 0.001$), drainage density (rho = -0.78, $p < 0.001$), and mean slope (rho = 0.71, $p < 0.001$). For Q95 ratio, basin relief shows the strongest correlation (rho = -0.58, $p < 0.001$), followed by developed fraction (rho = -0.34, $p = 0.015$) and mean elevation (rho = -0.34, $p = 0.018$). Flashiness index correlates with drainage area (rho = -0.42, $p = 0.003$) and drainage density (rho = 0.41, $p = 0.005$). The coefficient of variation of annual peaks shows a different pattern: forest fraction is the strongest correlate (rho = -0.55, $p < 0.001$), followed by Ksat (rho = -0.41, $p = 0.004$). Of the 77 feature-target pairs examined, 22 are significant at $p < 0.05$.

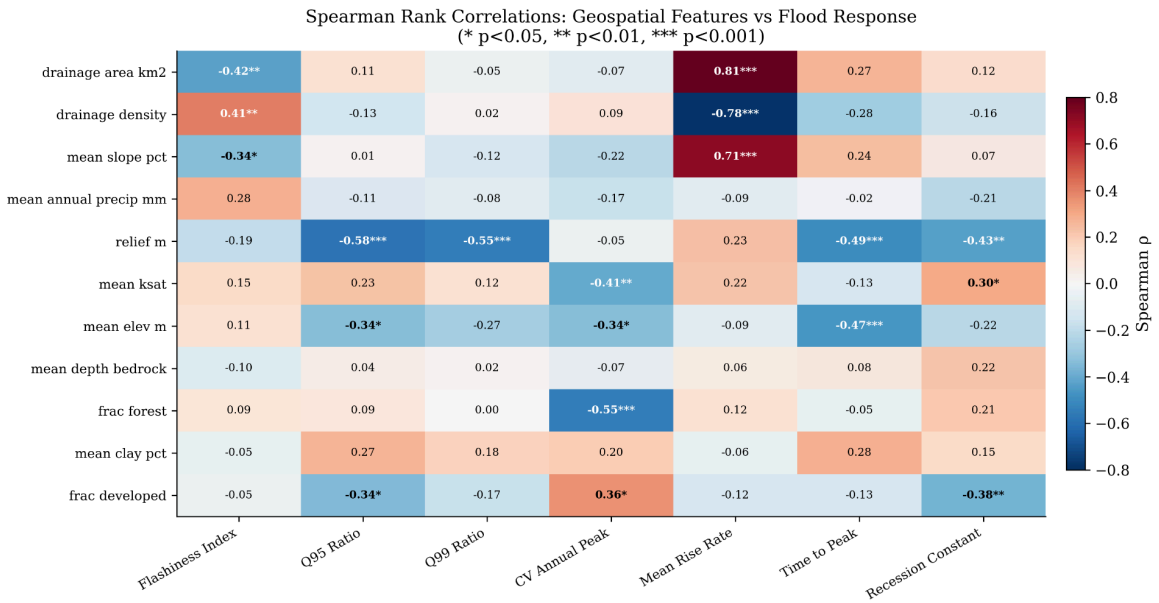

Figure 3. Spearman rank correlation heatmap between 11 geospatial features and 7 flood response targets. Asterisks indicate significance levels (* $p < 0.05$, ** $p < 0.01$, *** $p < 0.001$).

4.3 Machine Learning Model Performance

Mean rise rate is the most predictable target, with ElasticNet achieving R-squared = 0.73, followed by Ridge (0.73), XGBoost (0.67), and Random Forest (0.59). Q95 ratio is the second most predictable target, with XGBoost achieving R-squared = 0.33. Flashiness index and coefficient of variation of annual peaks are not predictable from static geospatial descriptors; all models produce negative or near-zero R-squared values. Tree-based models outperform Ridge in 5 of 7 targets, though the margin is small for the most predictable targets.

4.4 Gaussian Process Regression Results

GPR provides the best performance for 4 of 7 targets (Figure 4). For Q95 ratio, GPR with a Matern 1.5 kernel achieves R-squared = 0.46, a 40 percent improvement over XGBoost (R-squared = 0.33). For Q99 ratio, GPR with an RBF plus linear kernel achieves R-squared = 0.28. For mean rise rate, GPR with Matern 1.5 achieves R-squared = 0.73. For recession

constant, GPR with Matern 2.5 achieves R-squared = 0.24. The Matern 1.5 kernel, which models rough functions, performs best for Q95 ratio and mean rise rate. The RBF plus linear kernel performs best for Q99 ratio, indicating that a linear trend with smooth nonlinear deviations characterizes the relationship for extreme floods.

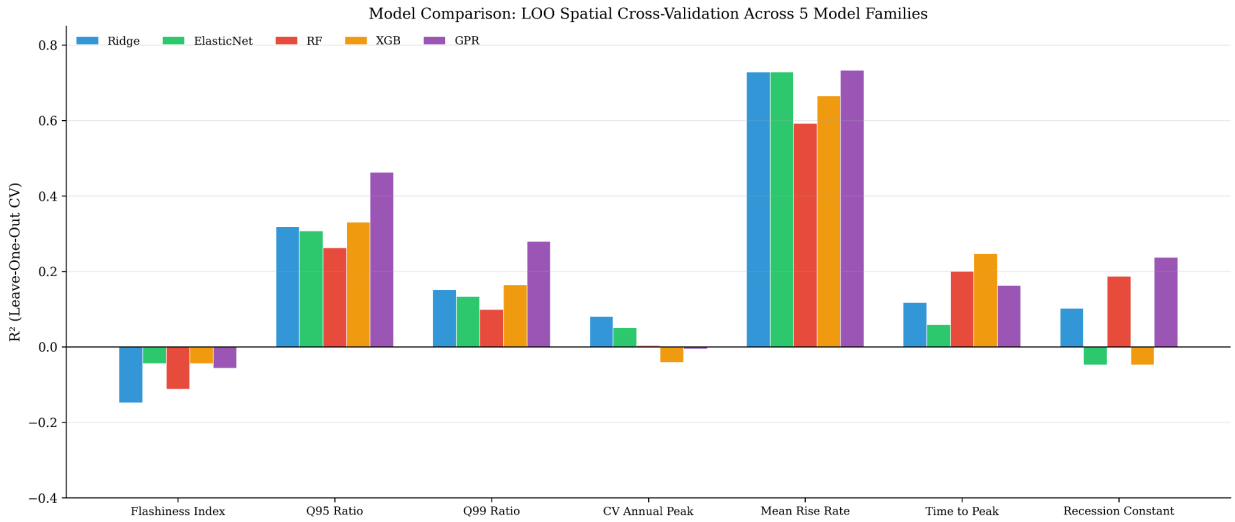

Figure 4. Model comparison showing R-squared values from leave-one-out spatial cross-validation across five model families and seven flood response targets.

4.5 Uncertainty Calibration

GPR prediction intervals show well-calibrated uncertainty (Figure 5). For Q95 ratio, the observed 95 percent prediction interval coverage is 91 percent. For mean rise rate, the coverage is 88 percent. For Q99 ratio, the coverage is 94 percent. For recession constant, the coverage is 95 percent. The normalized prediction interval widths range from 0.33 (mean rise rate) to 0.81 (Q99 ratio).

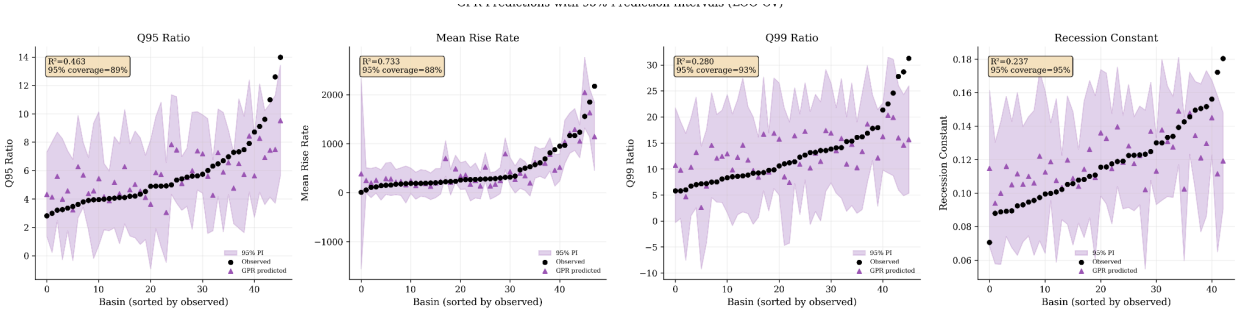

Figure 5. GPR predictions with 95 percent prediction intervals for the four targets with positive predictive skill. Black circles: observed values; purple triangles: GPR predictions; shaded bands: 95 percent prediction intervals.

4.6 SHAP Feature Importance

SHAP analysis reveals target-specific patterns (Figure 6). For Q95 ratio, terrain features dominate: relief accounts for 42 percent of total SHAP importance, followed by mean elevation (23 percent) and developed fraction (22 percent). For mean rise rate, morphometric features dominate: drainage area (39 percent) and drainage density (33 percent) account for 72 percent. For recession constant, relief is the leading feature (43 percent), followed by developed fraction (27 percent). For CV annual peak, forest fraction dominates (51 percent), a pattern that differs from all other targets.

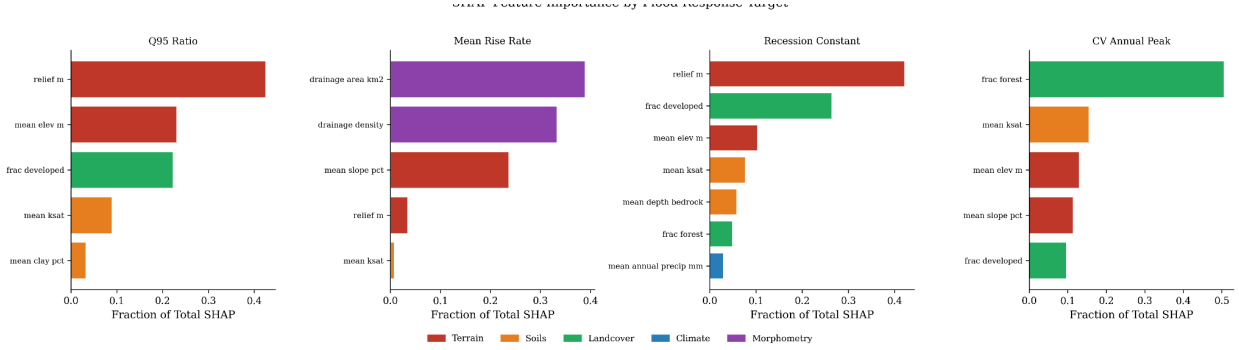

Figure 6. SHAP feature importance by flood response target, colored by geospatial feature group (terrain, soils, land cover, climate, morphometry).

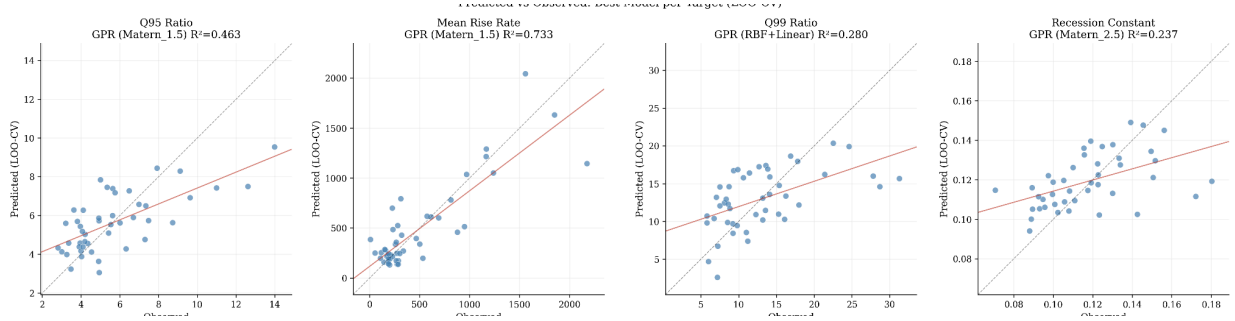

Figure 7. Predicted versus observed values for the best model per target using leave-one-out cross-validation. Dashed line: 1:1 line; red line: linear regression fit.

4.7 Hypothesis Test Results

Three of six hypotheses are supported. H1: slope correlates with flashiness (rho = -0.34, p = 0.018, supported). H4: larger basins are less flashy (rho = -0.42, p = 0.003, supported). H6: tree-based ML outperforms Ridge in the majority of targets (5 of 7, supported). Three hypotheses are not supported. H2: forest reduces flashiness (rho = 0.09, p = 0.54). H3: higher Ksat reduces flashiness (rho = 0.15, p = 0.31). H5: more clay increases flashiness (rho = -0.05, p = 0.74).

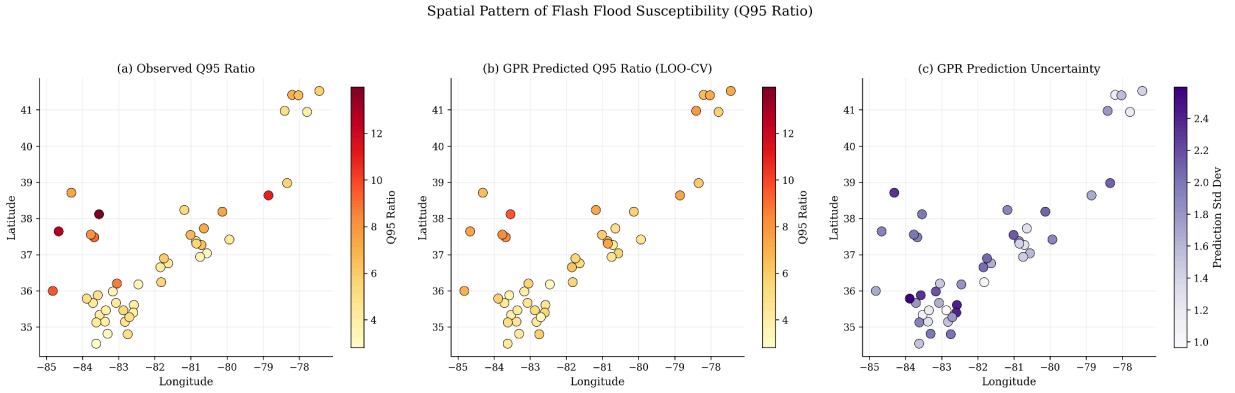

Figure 8. Spatial pattern of flash flood susceptibility (Q95 ratio): (a) observed values, (b) GPR predicted values from leave-one-out cross-validation, (c) GPR prediction uncertainty (standard deviation).

5. Discussion

5.1 Geospatial Predictability of Flood Response

The results show that geospatial basin descriptors can predict some flood response characteristics but not others. Mean rise rate (R-squared = 0.73) and Q95 ratio (R-squared = 0.46) are the most predictable targets. Flashiness index (R-squared less than 0) and CV annual peak (R-squared less than 0.1) are not predictable from static descriptors. Rise rate and Q95 ratio measure the magnitude of flood response, which is determined by the physical capacity of a basin to generate and concentrate runoff. Flashiness measures the frequency and rapidity of flow changes over time, which depends on the temporal characteristics of storm events as much as on basin properties. This interpretation is consistent with the finding of Gannon et al. (2022) that flashiness is not well organized by physical basin properties at continental scales.

5.2 The Role of Terrain

Terrain features, particularly relief and elevation, emerge as the dominant predictors for most flood response targets. Relief is the single most important feature for Q95 ratio (42 percent of SHAP), Q99 ratio, time to peak, and recession constant. This result aligns with established understanding of Appalachian flood hydrology: basins with greater relief have steeper hillslopes, thinner soils, and faster concentration times (Smith et al., 2011; Wooten et al., 2008).

The negative correlation between relief and Q95 ratio (rho = -0.58) may reflect the relationship between relief and basin size in this dataset. Basins with greater relief tend to be larger, and larger basins have lower Q95 ratios because their median discharge is higher relative to their peaks. When rise rate is examined, the correlation with slope is positive (rho = 0.71), confirming that steeper basins respond more aggressively to rainfall.

5.3 Land Cover and Soil Controls

Forest fraction shows no significant correlation with flashiness (rho = 0.09, p = 0.54), contradicting the common expectation that forest cover reduces flood response (Bradshaw et al., 2007). However, forest fraction does correlate with CV annual peak (rho = -0.55, $p < 0.001$), suggesting that forest cover stabilizes interannual flood variability even if it does not reduce flashiness on an event basis. This distinction between event-scale and interannual-scale flood behavior has not been highlighted in previous Appalachian flood studies.

Soil properties show limited predictive power for most targets. Ksat correlates with CV annual peak (rho = -0.41, p = 0.004) and recession constant (rho = 0.30, p = 0.037) but not with flashiness, Q95, or Q99. Depth to bedrock shows no significant correlation with any target, which may reflect the limitations of point-queried SSURGO data rather than distributed soil mapping.

5.4 Model Selection for Small-Sample Prediction

Regularized linear models perform comparably to tree-based models for most targets at this sample size (n approximately equal to 50). GPR provides the best overall performance, improving R-squared from 0.33 to 0.46 for Q95 ratio. The Bayesian framework of GPR is well suited to the small-sample regime because it regularizes through the prior and provides calibrated prediction intervals. For operational applications at ungauged sites, the combination of GPR predictive means and calibrated uncertainty intervals provides a more useful output than point predictions alone.

5.5 Complementarity with Temporal Forecasting

This study and the companion study (Bhattarai, 2026) address complementary aspects of the Appalachian flood prediction problem. The companion study demonstrated that ML models can forecast discharge at gauged stations with NSE = 0.90 at 2-hour lead time. The present study shows that geospatial features can predict flood magnitude indicators at ungauged sites with R-squared = 0.46. Together, the two studies cover the prediction needs for both gauged and ungauged basins. In both cases, SHAP reveals physically interpretable feature hierarchies that match hydrological theory.

5.6 Limitations

This study has several limitations. First, the sample size of 49 basins constrains the complexity of models that can be trained without overfitting. Second, the geospatial feature extraction used estimated basin extents rather than delineated watershed boundaries for many stations, introducing noise. Third, soil properties were queried at point locations rather than averaged across the contributing watershed. Fourth, the study does not include dynamic predictors such as antecedent soil moisture or storm event characteristics. Fifth, the climate variable was estimated using an elevation-based model for some stations. "Crow et al. (2017) demonstrated that pre-storm soil moisture conditions derived from SMAP are correlated with storm-event runoff ratio, which suggests that incorporating satellite soil moisture as a dynamic predictor could improve prediction of flashiness and other event-scale flood metrics that static geospatial descriptors fail to capture in this study."

6. Conclusions

This study evaluated whether geospatial basin descriptors can predict flash flood response characteristics at ungauged Appalachian watersheds. The analysis covered 49 USGS stations across seven states, 11 predictor variables, seven flood response targets, and five model families. The main findings are as follows.

First, geospatial predictors explain a moderate fraction of the variance in flood magnitude indicators (Q95 ratio R-squared = 0.46, mean rise rate R-squared = 0.73) but cannot predict flashiness index or interannual peak variability. Static landscape properties control how large floods get in a basin but not how often or how fast flow changes occur.

Second, terrain relief is the single most important predictor for most flood response targets, accounting for 42 to 43 percent of SHAP importance. Forest fraction is the dominant predictor for interannual peak variability (51 percent of SHAP). The geospatial controls on flood response are target-specific.

Third, Gaussian Process Regression with Matern kernels provides the best predictive performance for 4 of 7 targets and produces well-calibrated uncertainty estimates with 88 to 95 percent coverage of 95 percent prediction intervals.

Fourth, forest fraction does not correlate with flashiness (rho = 0.09, $p = 0.54$) but does correlate with reduced interannual peak variability (rho = -0.55, $p < 0.001$). This distinction has practical implications for forest management as a flood mitigation strategy.

Future work should expand the station network using CAMELS or GAGES-II datasets, incorporate satellite-derived dynamic predictors, and test graph neural network architectures.

Acknowledgements

Streamflow data were provided by the USGS National Water Information System. Terrain data were obtained from the USGS 3D Elevation Program. Land cover data were obtained from the Multi-Resolution Land Characteristics Consortium. Soil data were accessed through the NRCS Soil Data Access service. Climate data were obtained from the PRISM Climate Group at Oregon State University.

Funding Statement

This research received no external funding.

Data Availability Statement

All input data used in this study are publicly available. USGS streamflow records: https://waterdata.usgs.gov/nwis. 3DEP elevation data: https://www.usgs.gov/3d-elevation-program. NLCD land cover: https://www.mrlc.gov/data. SSURGO soils: https://sdmdataaccess.sc.egov.usda.gov. PRISM climate normals: https://prism.oregonstate.edu. Code and trained models will be archived at a public repository prior to publication.

Conflict of Interest

The author declares no conflict of interest.

References

Ashley, S. T., and Ashley, W. S. (2008). Flood fatalities in the United States. Journal of Applied Meteorology and Climatology, 47(3), 805-818.

Aydin, H. E., and Iban, M. C. (2023). Predicting and analyzing flood susceptibility using boosting-based ensemble machine learning algorithms with SHapley Additive Explanations. Natural Hazards, 116(3), 2957-2991.

Baker, D. B., Richards, R. P., Loftus, T. T., and Kramer, J. W. (2004). A new flashiness index: Characteristics and applications to midwestern rivers and streams. JAWRA Journal of the American Water Resources Association, 40(2), 503-522.

Beven, K. (2016). Facets of uncertainty: Epistemic uncertainty, non-stationarity, likelihood, hypothesis testing, and communication. Hydrological Sciences Journal, 61(9), 1652-1665.

Beven, K. J., and Kirkby, M. J. (1979). A physically based, variable contributing area model of basin hydrology. Hydrological Sciences Bulletin, 24(1), 43-69.

Bhattarai, S. (2026). Persistence dominates, physics persists: Ensemble machine learning for flash flood forecasting across diverse Appalachian watersheds. Artificial Intelligence for the Earth Systems. (Under review).

Booth, D. B., and Jackson, C. R. (1997). Urbanization of aquatic systems: Degradation thresholds, stormwater detection, and the limits of mitigation. JAWRA Journal of the American Water Resources Association, 33(5), 1077-1090.

Bradshaw, C. J. A., Sodhi, N. S., Peh, K. S. H., and Brook, B. W. (2007). Global evidence that deforestation amplifies flood risk and severity in the developing world. Global Change Biology, 13(11), 2379-2395.

Calder, I. R. (1990). Evaporation in the Uplands. Wiley, Chichester, UK, 148 pp.

Carpenter, T. M., Sperfslage, J. A., Georgakakos, K. P., Sweeney, T., and Fread, D. L. (1999). National threshold runoff estimation utilizing GIS in support of operational flash flood warning systems. Journal of Hydrology, 224(1-2), 21-44.

Clark, R. A., Gourley, J. J., Flamig, Z. L., Hong, Y., and Clark, E. (2014). CONUS-wide evaluation of National Weather Service flash flood guidance products. Weather and Forecasting, 29(2), 377-392.

Daly, C., Halbleib, M., Smith, J. I., Gibson, W. P., Doggett, M. K., Taylor, G. H., Curtis, J., and Pasteris, P. P. (2008). Physiographically sensitive mapping of climatological temperature and precipitation across the conterminous United States. International Journal of Climatology, 28(15), 2031-2064.

Dewitz, J. (2023). National Land Cover Database (NLCD) 2021 Products. U.S. Geological Survey data release. https://doi.org/10.5066/P9JZ7AO3.

Dunne, T., and Leopold, L. B. (1978). Water in Environmental Planning. W.H. Freeman, New York, 818 pp.

Ellison, D., et al. (2017). Trees, forests and water: Cool insights for a hot world. Global Environmental Change, 43, 51-61.

Falcone, J. A. (2011). GAGES-II: Geospatial Attributes of Gages for Evaluating Streamflow, version II. U.S. Geological Survey, Reston, VA.

Gannon, J. P., Kelleher, C. A., and Zimmer, M. A. (2022). Controls on watershed flashiness across the continental US. Journal of Hydrology, 609, 127713.

Gesch, D. B., Oimoen, M. J., and Evans, G. A. (2014). Accuracy assessment of the U.S. Geological Survey National Elevation Dataset, and comparison with other large-area elevation datasets: SRTM and ASTER. U.S. Geological Survey Open-File Report 2014-1008, 10 p.

Gourley, J. J., Erlingis, J. M., Hong, Y., and Wells, E. B. (2012). Evaluation of tools used for monitoring and forecasting flash floods in the United States. Weather and Forecasting, 27(1), 158-173.

Gourley, J. J., et al. (2017). The FLASH project: Improving the tools for flash flood monitoring and prediction across the United States. Bulletin of the American Meteorological Society, 98(2), 361-372.

Hrachowitz, M., et al. (2013). A decade of Predictions in Ungauged Basins (PUB): A review. Hydrological Sciences Journal, 58(6), 1198-1255.

Kohanpur, A. H., et al. (2023). Urban flood modeling: Uncertainty quantification and physics-informed Gaussian processes regression forecasting. Water Resources Research, 59(4), e2022WR033939.

Kratzert, F., Klotz, D., Shalev, G., Klambauer, G., Hochreiter, S., and Nearing, G. (2019). Towards learning universal, regional, and local hydrological behaviors via machine learning applied to large-sample datasets. Hydrology and Earth System Sciences, 23(12), 5089-5110.

Lundberg, S. M., and Lee, S. I. (2017). A unified approach to interpreting model predictions. Advances in Neural Information Processing Systems, 30, 4765-4774.

Lundberg, S. M., et al. (2020). From local explanations to global understanding with explainable AI for trees. Nature Machine Intelligence, 2(1), 56-67.

Nearing, G., et al. (2024). Global prediction of extreme floods in ungauged watersheds. Nature, 627, 559-563.

NOAA NCEI (2024). Billion-Dollar Weather and Climate Disasters. https://www.ncei.noaa.gov/access/billions/.

Pradhan, B., Lee, S., Dikshit, A., and Kim, H. (2023). Spatial flood susceptibility mapping using an explainable artificial intelligence (XAI) model. Geoscience Frontiers, 14(6), 101625.

Ries, K. G., III, et al. (2017). StreamStats, version 4. U.S. Geological Survey Fact Sheet 2017-3046.

Rojas Aldana, S., Vergara, H., and Gourley, J. J. (2021). Toward predicting flood event peak discharge in ungauged basins. Journal of Hydrometeorology, 22(11), 2971-2988.

Sivapalan, M., et al. (2003). IAHS decade on Predictions in Ungauged Basins (PUB), 2003-2012. Hydrological Sciences Journal, 48(6), 857-880.

Smith, J. A., Baeck, M. L., Villarini, G., Wright, D. B., and Krajewski, W. (2011). Extreme flood response: The June 2008 flooding in Iowa. Journal of Hydrometeorology, 12(5), 862-879.

Soil Survey Staff (2020). Gridded Soil Survey Geographic (gSSURGO) Database. USDA NRCS.

Sun, A. Y., Wang, D., and Xu, X. (2014). Monthly streamflow forecasting using Gaussian Process Regression. Journal of Hydrology, 511, 72-81.

Tao, K., and Barros, A. P. (2013). Using fractal downscaling of satellite precipitation products for hydrometeorological applications. Journal of Atmospheric and Oceanic Technology, 30(3), 409-425.

USGS (2024). National Water Information System (NWIS). https://waterdata.usgs.gov/nwis.

Wolock, D. M., and McCabe, G. J. (1995). Comparison of single and multiple flow direction algorithms for computing topographic parameters in TOPMODEL. Water Resources Research, 31(5), 1315-1324.

Woods, D., et al. (2023). Hydrologic evaluation of the Global Precipitation Measurement Mission over the U.S. Journal of Hydrology, 619, 129124.

Wooten, R. M., et al. (2008). Frequency and magnitude of selected historical landslide events in the southern Appalachian Highlands. NC Geological Survey Report of Investigations, 30, 32 p.

Vieux, B.E. (2016). Geospatial Data for Hydrology. In: Distributed Hydrologic Modeling Using GIS. Water Science and Technology Library, vol 74. Springer, Dordrecht. https://doi.org/10.1007/978-94-024-0930-7_2

Crow, W. T., Chen, F., Reichle, R. H., and Liu, Q. (2017). L band microwave remote sensing and land data assimilation improve the representation of prestorm soil moisture conditions for hydrologic forecasting. Geophysical Research Letters, 44(11), 5495-5503.

Gonzales-Inca, C., Calle, M., Croghan, D., Torabi Haghighi, A., Marttila, H., Silander, J., and Alho, P. (2022). Geospatial Artificial Intelligence (GeoAI) in the Integrated Hydrological and Fluvial Systems Modeling: Review of Current Applications and Trends. Water, 14(14), 2211.